Graphene-Draped Semiconductors for Enhanced Photocorrosion Resistance and Photocatalytic Properties

Mengye Wang,[1] Lejuan Cai,[1] Yi Wang,[1] Feichi Zhou,[1] Kang Xu,[1] Xiaoming Tao,[2] and Yang Chai[1]*

[1]Department of Applied Physics, The Hong Kong Polytechnic University, Hung Hom, Kowloon, Hong Kong, People's Republic of China

[2]Institue of Textiles & Clothing, The Hong Kong Polytechnic University, Hung Hom, Kowloon, Hong Kong, People's Republic of China

KEYWORDS: Graphene, CdS semiconductor photocatalyst, anti-photocorrosion, photocatalytic performance, DFT calculations

ABSTRACT: Semiconductor photocatalysts have been widely used for photochemical water splitting, purification of organic contaminants, and bacterial detoxification. However, most photocatalysts suffer greatly from photocorrosion under visible light irradiation. Here we report a viable strategy to markedly improve photocorrosion resistance of photocatalysts by draping ultrathin yet highly impermeable graphene layers over a semiconductor CdS electrode. Remarkably, the average lifetime of three-layer-graphene-draped CdS photocatalyst is prolonged by 8 times compared to as-prepared CdS counterpart without graphene draping. The introduction of graphene layers largely suppresses the charge carrier recombination of CdS film and decreases the carrier transfer resistance at the graphene-draped CdS electrode/electrolyte interface, as revealed by the photoluminescence (PL) and electrochemical impedance spectroscopy studies, respectively, thereby leading to increased photocurrent and enhanced photocatalytic performance (i.e., a 2.5-fold increase in comparison to that in as-prepared CdS case). Our density functional theory calculations also show that electrons are readily transferred from CdS to graphene, correlating well with the PL measurement. The photocorrosion is mainly caused by oxidation reaction between CdS and O_2 and H_2O assisted with photo-generated holes, evidenced by X-ray photoelectron spectroscopy characterization. The draped graphene effectively prevents the direct contact between CdS film and O_2 and H_2O, thus considerably retarding the photocorrosion of CdS upon visible light exposure. This simple yet robust graphene-draping strategy for anti-photocorrosion of semiconductor photocatalysts is environmentally friendly as it prevents them from entering into surrounding environment, thus eliminating the possible secondary pollution.

Introduction

Photocorrosion is an oxidation or reduction process of photocatalysts, which originates from the photogenerated electrons/holes, and the interaction of photogenerated electrons/holes with the surrounding media such as O_2 and H_2O, or concurrent occurrence of both events.[1] As a result of photocorrosion, the lifetime and performance of photocatalysts are significantly decreased over a long course of photocatalysis. Clearly, breakthrough strategies are required to greatly improve the stability of photocatalysts and advance the use of unstable yet highly efficient semiconductors in photochemical hydrogen generation,[2] photochemical degradation of organic pollutants and toxic compounds,[3] and organic fuels production.[4] In this context, three commonly used anti-photocorrosion approaches have been developed.[5-7] The first two approaches involve mixing photocatalyst with another material to prevent photoactive catalyst from reacting with photo-induced electrons/holes by rapidly transferring charge carriers through this added material,[6] and consuming these photo-induced charge carriers by sacrificial agents,[5,8] respectively. However, these approaches require either the exposure of catalysts to the ambient environment or the continuous addition of sacrificial agents. The third approach is to physically reduce the possible contact between photocatalyst and the ambient environment by depositing a thin layer of protecting material over photocatalyst.[7] Nevertheless, the thickness of coated layer is usually at least a few nanometers,[7] which reduces the optical absorption of photocatalysts and increases the carrier transport path of

photocatalysts to their active sites on the surface. Clearly, it is highly desirable to deposit a thin yet transparent and stable layer on the surface of unstable semiconductor photocatalysts to greatly improve their anti-photocorrosion performance.

Among various types of photocatalysts, semiconductor CdS possesses excellent photocatalytic performance due to its relatively narrow band gap (~2.4 eV) and appropriate band position that meets the thermodynamic requirement for photocatalysis applications.[9] However, CdS has relatively low chemical stability under visible light irradiation as it can be easily oxidized by O_2 and H_2O from the ambient environment.[1] To date, several methods have been developed to retard the photocorrosion of CdS nanoparticles (NPs), such as coupling CdS NPs with a hole-conducting material to reduce the oxidation caused by photo-generated holes,[10] wrapping CdS NPs with a thin layer of wide bandgap semiconductor to decrease the oxidation of CdS resulted from the ambient condition,[11] and enabling photo-induced holes to react with either the added sacrificial agents[12] or the electrons generated in a Z-scheme photocatalytic system.[13,14] However, most of these methods often invoke harsh synthesis conditions or require continuous feeding of sacrificial agents into photocatalytic system. Moreover, these works noted above focused on CdS NPs. In contrast, the study on efficiently inhibiting the photocorrosion of CdS electrodes is relatively few and limited in scope.

Herein, we report a facile and effective strategy to markedly improve anti-photocorrosion properties of CdS photocatalysts by judiciously draping ultrathin graphene with proper number of layers over CdS film. Due to high optical transmittance, excellent conductance, and high impermeability of graphene,[15-23] the advantages of exploiting graphene as protecting layer for CdS film are threefold. First, the thickness of graphene layer is at the atomic level. In sharp contrast to the deposition of metal or semiconductor layer on the surface of CdS electrode, the draping of thin graphene layers enables an impressively high optical transmittance (*e.g.,* more than 92% for three layers of graphene),[24,25] and thus favors the light absorption of CdS. Moreover, thin graphene layer facilitates a rapid charge carrier transfer from CdS to graphene, thereby effectively reducing the recombination of charge carriers. Second, thin graphene layer functions as an ideal barrier as the pore size of its honeycomb-like carbon lattices (0.064 nm) is smaller than the van der Waals radii of the smallest atoms, thus blocking the direct contact of CdS with the surrounding media (*e.g.*, H_2O and O_2.) by preventing the passage of these small molecules.[26,27] In this study, compared with as-prepared CdS electrode, the three-layer-graphene-draped CdS electrode exhibits an eightfold increase in the effective lifetime under visible light irradiation. Lastly, the introduction of graphene layers promotes the charge carrier separation of CdS and the carrier transport at the graphene-draped CdS electrode/electrolyte interface, as evidenced by photoluminescence (PL) and electrochemical impedance spectroscopy (EIS) measurements, respectively. Consequently, the enhanced photocurrent and increased photocatalytic performance are achieved by capitalizing on these graphene-draped CdS electrodes. For example, a 2.5-time improvement in photoelectrocatalytic efficiency was found by using a three-layer-graphene-draped CdS electrode. The photocorrosion induced by oxidation reaction between CdS and O_2 and H_2O and the important role of graphene in preventing photocorrosion of CdS by blocking O_2 and H_2O molecules from contacting with CdS are scrutinized by XPS measurements and DFT calculations, respectively.

Methods

Fabrication of graphene-draped CdS photocatalyst. Fluorine-doped tin oxide (FTO)-coated glass substrates were sequentially ultrasonically cleaned using acetone, isopropyl alcohol, and distilled water, and then blow-dried with N_2. Subsequently, CdS film was electrodeposited onto the FTO glass substrate in a two-electrode system cell (FTO glass as the working electrode and Pt foil as the counter electrode) under a constant current density of -0.5 mA cm^{-2} for 3.5 min at room temperature.[28] The electrolyte was a DMSO solution containing 0.01 M $Cd(NO_3)_2$ and 0.02 M S. After electrodeposition, as-prepared CdS electrode was immersed in acetone for 30 s, and then blow-dried with N_2.

Monolayer graphene grown on the copper foil was purchased from Vigon Technologies Co., Ltd. A thin layer of poly(methyl methacrylate) (PMMA) was spin-coated (500 rpm for 5 s and 3000 rpm for 30 s) on graphene as the supporting layer. The copper foil was then etched in the ammonium peroxydisulfate solution. Double and triple layers of graphene (denoted 2LG or 3LG) were obtained via a layer-by-layer transfer method. Subsequently, the PMMA-coated graphene was transferred onto the surface of CdS electrode, followed by annealing CdS/graphene photocatalyst at 65 °C in order to increase the adhesion between CdS and graphene. Finally, PMMA on the surface of graphene was removed by acetone. Nail polish was used to fix and define the effective area of graphene-draped CdS photocatalysts.

Characterizations. The morphology and crystal structure of CdS were characterized by scanning transmission electron microscope (STEM, Jeol JEM-2100F). The optical transmittance of different layers of graphene was assessed by UV-vis spectrophotometer (Shimadzu, UV-2550). The composition and crystal structure of CdS and graphene-draped CdS were measured by Raman spectroscope (Horiba HR800) with an excitation wavelength of 488 nm. Photoluminescence (PL) spectra of CdS and graphene-draped CdS were examined by fluorescence spectrophotometer (Hitachi F-7000, λ_{ex} = 380 nm). The potentiostatic measurement and electrochemical impedance spectroscopy (EIS) of CdS and graphene-draped CdS were performed using Solartron Analytical in a three-electrode configuration consisting of a working electrode (as-prepared sample), a counter electrode (Pt foil) and a reference electrode (saturated calomel electrode, SCE) in 0.1 M Na_2SO_4.

Visible light was provided by a tungsten-halogen lamp (500 W with a light intensity of 100 mW cm^{-2}). The same light source and light intensity were used in photocatalytic measurements described below. The composition of samples was obtained by using X-ray photoelectron spectroscopy (XPS, Thermol Scientific Escalab 250Xi, Al Kα radiation).

The photocatalytic activity was evaluated using the same three-electrode system as noted above in a quartz glass reactor with a water jacket to keep reaction at room temperature. 5 mg L^{-1} Rhodamine B (RhB) aqueous solution was used as a target pollutant. A negative bias potential (-0.3 V *vs* saturated calomel electrode, SCE) was applied on CdS and graphene-draped CdS. During the photocatalytic test, an electrode photocatalyst (CdS or graphene-draped CdS) was immersed in the vigorously stirred RhB solution. The change of RhB concentration was monitored by UV-vis spectrophotometer (Shimadzu, UV-2550) at the wavelength of 557 nm at a 30-min interval.

Simulation. Theoretical calculations of charge density difference were performed using density functional theory (DFT) by implementing VASP code with exchange-correlation energy function that is modeled by Perdew-Burke-Ernzerhof (PBE) function.[29] The (1×1) surface with a cut-off energy of 520 eV was applied to determine a reliable thickness for simulating a bulk-like CdS slab. Considering the lattice matching, a (3×3) supercell was used to construct a CdS/graphene complex surface with the exposed Cd as the final model because of the minimal surface energy of CdS. The K-points were 5 × 5 × 1 for bulk CdS and 3 × 3 × 1 for the graphene-draped CdS supercell, respectively. The thickness of vacuum in all systems (CdS/1LG and CdS/2LG, where 1LG and 2LG represent one layer and two layers of graphene) was set to 30 Å in z-axis in order to eliminate the interaction of nearby slabs caused by the periodic boundary condition. During the geometry optimization, all structures were relaxed to an energy convergence of 10^{-5} eV/atom and a force convergence of 0.01 eV/Å.

The barrier energies of graphene to O_2 and H_2O molecules were obtained by Quantum Espresso (QE) code. The generalized gradient approximation (GGA) Perdew-Burke-Ernzerhof (PBE) exch-corr was selected as the pseudopotential functional type. The graphene layers with no vacancy, divacancy and eight-atom vacancy were calculated. The distance between the graphene plane and O_2 (or H_2O) molecule is varied from 3.7 Å to 0 Å. Each system contains at least a 20-Å vacuum region in z-axis to prevent the influence from the neighbor slabs. The convergence threshold on total energy is 10^{-6} a.u. and the one on forces is 10^{-3} a.u.. The kinetic energy cutoff for wave functions is 50 Ry (Rydberg unit of energy, 1 Ry = 13.6 eV), and the kinetic energy cutoff for charge density and potential is 200 Ry.

Results and Discussions

A schematic of CdS electrode draped with three layers of graphene (denoted CdS/3LG) is illustrated in **Figure 1a**. First, as-prepared CdS electrode (i.e., without graphene draping) was characterized. High-resolution TEM measurement on as-prepared CdS film shows a lattice fringe of 0.33 nm, corresponding to the reflection from the (111) plane of cubic CdS (**Figure 1b**). The selected area electron diffraction (SAED) measurement suggests that CdS film is polycrystalline (**Figure S1b**). The three diffraction rings are indexed to (111), (220) and (311) planes of cubic CdS, respectively. A monolayer graphene (denoted 1LG) reaches a light transmittance of 97% (**Figure 1c**). A 92% light transmittance is retained for a three-layer graphene (3LG) (**Figure 1c**), which is consistent with the reported results.[24] **Figure 1d** compares the Raman spectra of CdS draped with different layers of graphene. Three peaks at 300.7 cm^{-1}, 598.2 cm^{-1} and 899.0 cm^{-1} agree well with 1LO, 2LO and 3LO Raman peaks of CdS.[30] The Raman-active modes of hexagonal CdS (*i.e.,* E_2 at 43 cm^{-1}, A_1(TO) at 234 cm^{-1}, E_2 at 256 cm^{-1}, E_1(TO) at 243 cm^{-1}, A_1(TO) at 305 cm^{-1}, and E_1(LO) at 307 cm^{-1}) are not observed, suggesting a cubic-phase CdS.[30,31] Additionally, the intensity ratio of I_{2LO}/I_{1LO} has a low value of ~0.26 (**Figure S1c**), further confirming cubic structure of CdS.[32] The appearance of characteristic G and 2D peaks and the absence of the D peak of graphene signify the high quality of graphene layer(s) (**Figure S1d**).[33] The intensity ratios of I_{2D}/I_G are 1.73, 1.01, and 0.21, which correlate well with one, two, and three layers of graphene, respectively, on the surface of CdS film (**Figure S1d**).[34,35]

The lifetimes of as-prepared CdS and graphene-draped CdS films were estimated by measuring the photocurrents as a function of time upon the exposure to visible light (see *Methods*) without applying a bias potential (**Figure 2a**). The photocurrent of as-prepared CdS electrode drops to zero after a 20-min visible light irradiation, implying that CdS is rapidly photocorroded. In contrast, graphene-draped CdS electrodes (i.e., CdS/1LG, CdS/2LG, and CdS/3LG) still exhibit relatively high photocurrent densities at t = 20 min. Moreover, the digital images of these electrodes irradiated by visible light for a different amount of times further provide clear evidence that the graphene draping is of key importance in effectively improving the photocorrosion resistance of CdS (**Figure 2b**). Prior to visible light exposure, all samples display yellow color. After irradiation for 20 mins, the pristine CdS electrode without the graphene protection turns colorless, indicating that CdS is oxidized into SO_4^{2-} and then diffuses in the electrolyte.[1] At t = 20 min, the graphene-draped CdS electrodes remain yellowish (second column in **Figure 2b**). CdS/1LG, CdS/2LG, and CdS/3LG start to fade after 60-, 120-, and 180-min visible light irradiation, respectively.

As shown in **Figure 2a**, with the increasing number of graphene layers, the lifetimes of CdS are extended, which may be attributed to the enhanced impermeability by graphene draping. We set 0.5 μA cm^{-2} as the standard

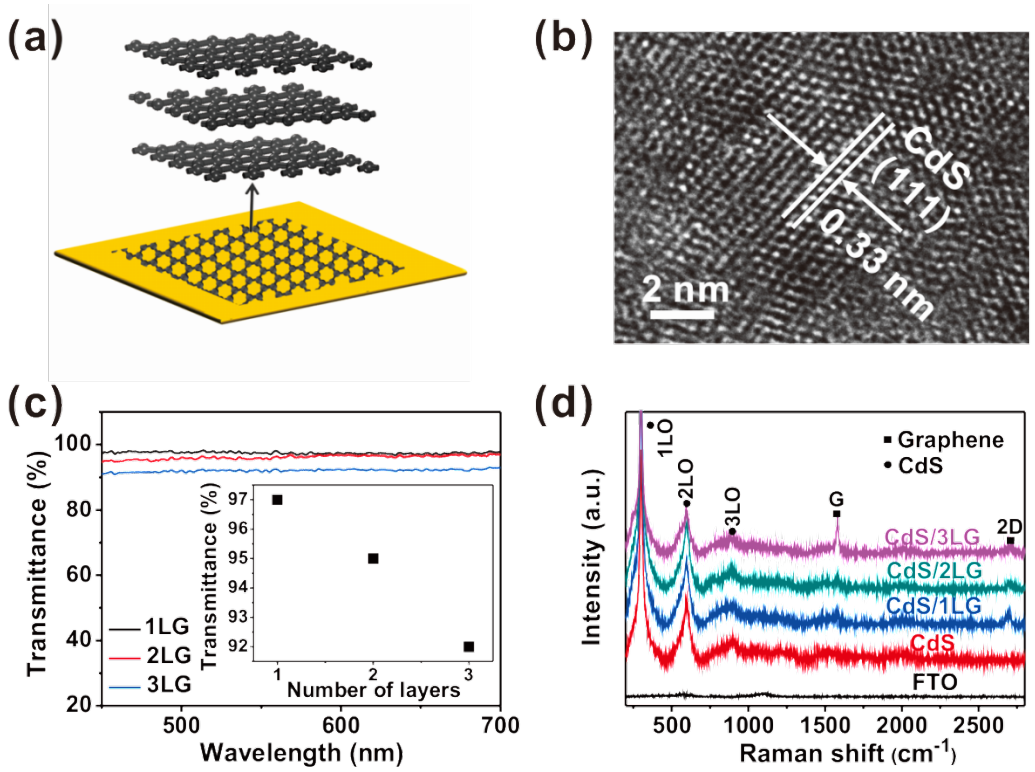

Figure 1. (a) Schematic illustration of CdS draped with three layers of graphene (denoted CdS/3LG). A close-up of three graphene layers is shown in the upper panel. (b) High resolution TEM image of as-prepared CdS electrode. (c) Transmittance spectra of three different layers of graphene. (d) Raman spectra of as-prepared CdS electrode and CdS electrodes covered with one, two and three layers of graphene (hereafter referred to as CdS/1LG, CdS/2LG, and CdS/3LG, respectively).

photocurrent density to compare the effective lifetimes of CdS and graphene-draped CdS electrodes as their photocatalytic activities are quite low below this value. For CdS, CdS/1LG, CdS/2LG and CdS/3LG electrodes, the times for photocurrent density decreasing to 0.5 μA cm^{-2} are roughly 11, 24, 46, and 88 min, respectively (**Figure 2a**). Thus, compared with as-prepared CdS, the lifetimes of CdS/1LG, CdS/2LG and CdS/3LG electrodes increase by approximately 2.2, 4.2, and 8.0 times, respectively, signifying the enhanced visible-light photocorrosion resistance after CdS films are draped with thin layers of graphene. The photocurrent density is resulted from the photo-generated charge carriers and the photocorrosion reaction of CdS. It is clear that at the beginning of irradiation (*i.e.*, from 0 to 7 min; **Figure 2a**), the photocurrent densities of CdS/1LG and CdS/2LG electrodes are considerably higher than that of as-prepared CdS electrode, which is possibly due to the improved separation of photoinduced charge carriers. It is also interesting to note that the photocurrent density of CdS/3LG electrode is lower than that of as-prepared CdS electrode during the first 2-min irradiation, suggesting that three layers of graphene draping effectively inhibits the oxidization of CdS by H_2O and O_2. Among three graphene-draped CdS samples, their current densities progressively decrease with the increased number of graphene layers and $I_{CdS/1LG} > I_{CdS/2LG} > I_{CdS/3LG}$ when visible light irradiation is less than 7 mins. This is not surprising as it is increasingly difficult for photo-generated charge carriers to transfer between the graphene interlayer. Interestingly, as the irradiation continues (i.e., after 7 mins), although the current densities decrease accordingly, the reversed trend (i.e., $I_{CdS/1LG} < I_{CdS/2LG} < I_{CdS/3LG}$ as the number of graphene layers increases) was seen. This observation suggests a trade-off between the photocorrosion resistance of semiconductor electrode and its photocatalytic activity in determining the proper number of graphene layers to be draped.

Figure 3a compares the PL spectra of CdS and graphene-draped CdS electrodes. The graphene-draped CdS samples display much lower PL intensities in comparison with as-prepared CdS, signifying the effectiveness of graphene draping in transferring photo-excited electrons from CdS to graphene and suppressing the recombination of photo-induced electrons and holes. This is due to the formation of barrier at the graphene/CdS interface[36,37] that prevents the back transfer of electrons (**Figure 3b**). Furthermore, the increase of graphene layer contributes to a higher potential difference at CdS/graphene interface, leading to a lowered PL intensity. The charge density distributions at the interface between CdS and graphene with different number of layers are revealed by density functional theory (DFT) calculations (**Figure 3c** and **Figure 3d**). It is notable that the Cd-exposed CdS experiences an electron depletion process after contacting with graphene, and an electron accumulation occurs on the graphene layer. The calculations clearly show that electro-

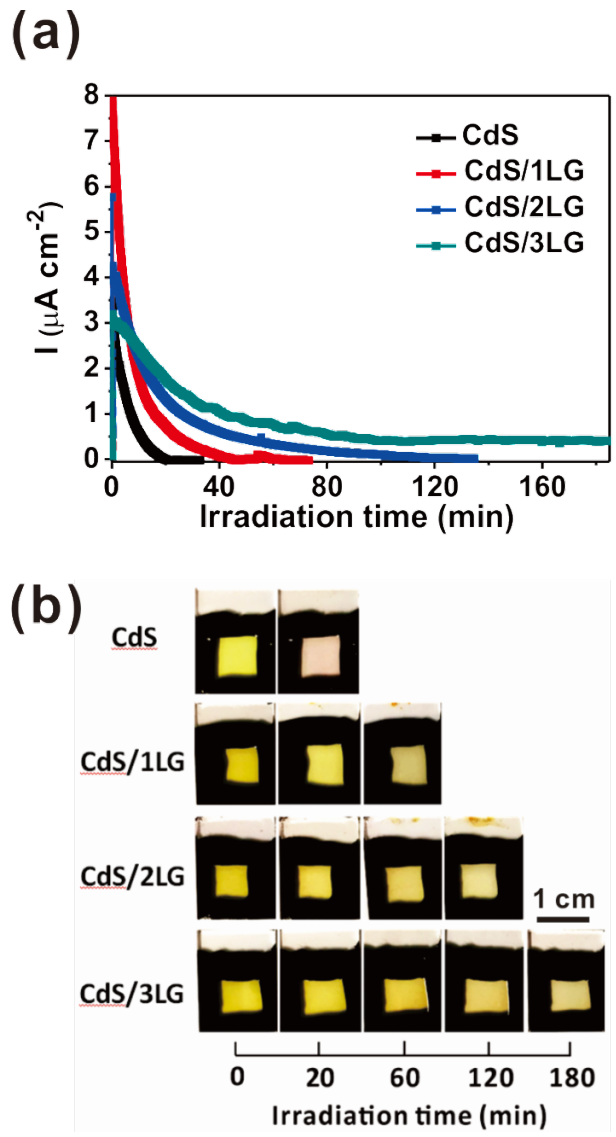

Figure 2. The lifetime measurements on as-prepared CdS, CdS/1LG, CdS/2LG, and CdS/3LG. (a) Potentiostatic curves. The applied bias potential was 0 V (*vs.* SCE). (b) Digital images of as-prepared CdS, CdS/1LG, CdS/2LG, and CdS/3LG taken at different visible light irradiation times. The yellow and black areas are the electrodeposited CdS on the FTO glass and the nail polish, respectively.

ns are readily transferred from CdS to graphene, which is in good agreement with the PL results (**Figure 3a**).

The interfacial properties between electrode photocatalysts and electrolyte were scrutinized by electrochemical impedance spectroscopy (EIS) measurements performed over a frequency range from 1×10^5 Hz to 0.1 Hz in the dark and under visible light irradiation (**Figure 3e**). The diameter of Nyquist plot at high frequency is correlated with the charge transfer process, reflecting the charge transfer resistance at the electrode/electrolyte interface. As shown in **Figure 3e** and **Table S1**, the graphene draping significantly reduces the interfacial charge transfer resistance (R_{ct}) and improves the charge transfer from electrode to electrolyte, suggesting a higher photocatalytic efficiency of graphene-draped CdS electrode. In addition, the R_{ct} increases with the increased number of graphene layers under visible light irradiation (**Table S1**) as less photo-induced charge carriers can reach the interface between electrode and electrolyte due to relatively difficult interlayer charge migration of graphene. This correlates well with the decrease of photocurrent density with the increased number of graphene layers (i.e., $I_{CdS/1LG} > I_{CdS/2LG} > I_{CdS/3LG}$) when irradiating for less than 7 mins as discussed above (**Figure 2a**).

The photoelectrocatalytic performances of CdS and graphene-draped CdS electrodes are evaluated by degrading Rhodamine B (RhB) under a bias potential of -0.3 V (*vs.* saturated calomel electrode, SCE). After visible light irradiation for 0.5 h, RhB is self-degraded by 0.05%, and in the meantime 1.81%, 2.82%, 4.02%, and 4.54% degradation of RhB are achieved by capitalizing on CdS, CdS/1LG, CdS/2LG, and CdS/3LG electrodes as photocatalysts, respectively (**Figure 3f**). Compared with as-prepared CdS electrode, graphene-draped CdS electrodes show the increased photocatalytic degradation of RhB due likely to the more effective separation of photogenerated electrons and holes and the faster charge transfer from electrode to electrolyte. It is important to note that the photocatalytic degradation ability of as-prepared CdS declines quickly and reaches a plateau after 30 mins, indicating that CdS is totally photocorroded (**Figure 2a**). In comparison to the case of CdS/1LG electrode in which the degradation of RhB remains nearly unchanged after 1 h, CdS/2LG and CdS/3LG electrodes exhibit high photocatalytic efficiencies and possess such high activities for 4 h or even longer. (**Figure 3f and Figure S3**) For the CdS/1LG sample, it is plausible that O_2 and H_2O may penetrate through the defects of monolayer graphene to oxidize the CdS film underneath under light irradiation. However, as the number of graphene layers increases, the upper graphene layer can cover the defects of the lower one, thereby improving the photocorrosion resistance. Furthermore, the applied negative bias potential (-0.3 V *vs* SCE) on these electrode photocatalysts effectively removes holes through the external circuit, thus reducing the hole-induced oxidization reactions. As as-prepared CdS is photocorroded after 30 min, the photocatalytic degradations of RhB by all samples within a 30-min visible light irradiation are fit by using a pseudo-first order kinetic model, $\ln(C/C_o) = |k|t$, where C_o and C are the concentrations of RhB prior to degradation and at time t, respectively, and $|k|$ is the pseudo-first-order degradation kinetic constant. As depicted in **Figure S2**, $|k|$ of CdS, CdS/1LG, CdS/2LG, and CdS/3LG are 6.08×10^{-4} min^{-1}, 9.53×10^{-4} min^{-1}, 1.37×10^{-3} min^{-1}, and 1.55×10^{-3} min^{-1}, respectively. Obviously, the photocatalytic activities of CdS/2LG and CdS/3LG photocatalysts are markedly enhanced, implying that the graphene layers not only isolate the CdS electrode from contacting with O_2 and H_2O in the ambient environment, but also decrease the recombination of photo-induced charge carriers of CdS by forming a barrier

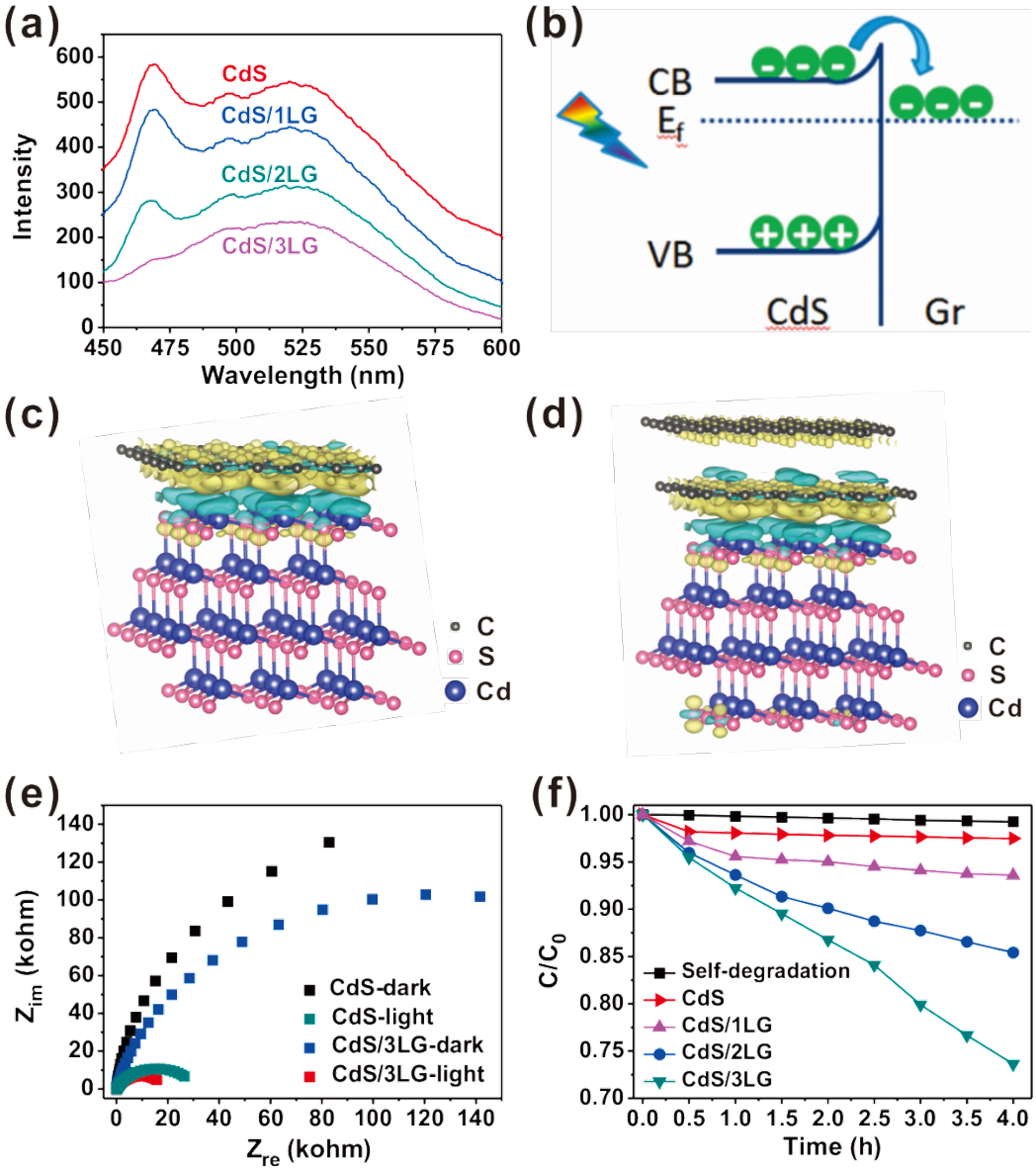

Figure 3. (a) Photoluminescence (PL) spectra of as-prepared CdS, CdS/1LG, CdS/2LG, and CdS/3LG, respectively. (b) Schematic illustration of the barrier formed at the CdS/graphene interface. Gr represents graphene. Charge density difference of (c) CdS/1LG and (d) CdS/2LG simulated using DFT calculation, respectively, where the yellow and blue isosurfaces represent the charge accumulation and depletion in the space, respectively. (e) Electrochemical impedance spectra (EIS) of CdS and CdS/3LG in the dark and under visible light irradiation. (f) Photocatalytic degradation of RhB under visible light irradiation as a function of time by employing as-prepared CdS, CdS/1LG, CdS/2LG, and CdS/3LG electrodes, respectively (I_o =100 mW cm^{-2}).

at the CdS/graphene interface (**Figure 3b**). Moreover, lower charge transfer resistance at the electrode/electrolyte interface (**Figure 3e** and **Table S1**) favors photocatalytic reactions. Taken together, a 2.5-fold increase ($1.55\times10^{-3}/(6.08\times10^{-4})=2.5$) of photocatalytic performance for CdS/3LG electrode is achieved in comparison with as-prepared CdS electrode.

The photocorrosion processes of CdS in the presence and absence of H_2O and O_2 can be described by equations (1) and (2), respectively.[38]

$$CdS + 4h^+ + 2H_2O + O_2 \rightarrow Cd^{2+} + SO_4^{2-} + 4H^+ \quad (1)$$

$$CdS + 2h^+ \rightarrow Cd^{2+} + S \quad (2)$$

where h^+ is the photo-generated holes of CdS.

In order to assess the difference in chemical composition of CdS with and without the graphene draping, X-ray photoelectron spectroscopy (XPS) measurements were carried out. Under visible light irradiation, photo-induced holes can readily oxidize CdS into SO_4^{2-} in the presence of H_2O and O_2 (equation 1). The SO_4^{2-} ions can then rapidly diffuse into the solution, thereby facilitating the continuous proceeding of oxidation reaction of CdS. After a 10-min irradiation, SO_4^{2-} ions are detected from as-prepared CdS sample (peaks at 169.1 eV and 167.9 eV, respectively; **Figure 4a**). Prior to visible light irradiation, the CdS/3LG

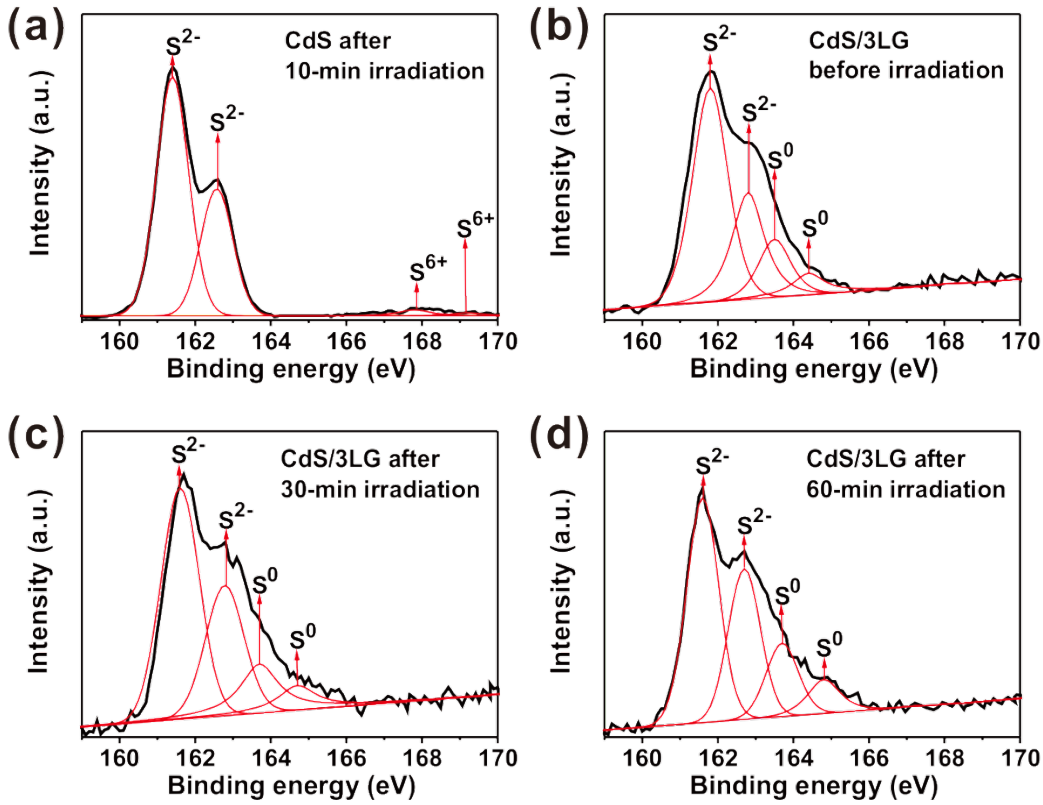

Figure 4. High-resolution X-ray photoelectron spectroscopy (XPS) spectra of S 2p for (a) as-prepared CdS electrode after a 10-min visible light irradiation, (b) CdS/3LG electrode prior to irradiation, (c) CdS/3LG electrode after a 30-min visible light irradiation, and (d) CdS/3LG electrode after a 60-min visible light irradiation.

sample is composed of Cd, S and C elements (**Figure S4**) and no SO_4^{2-} ions are observed (**Figure 4b**). Rather than the formation of SO_4^{2-}, as CdS is isolated from the ambient environment via the graphene draping, CdS is oxidized by photo-induced holes into S upon irradiation (equation 2; the spin-orbital photoelectrons of S^{2-} ($2p_{3/2}$ and $2p_{1/2}$) and S^0 ($2p_{3/2}$ and $2p_{1/2}$) at binding energies of 161.6 eV (for S^{2-}), 162.7 eV (for S^{2-}), 163.6 eV (for S^0), and 164.7 eV (for S^0), respectively; **Figure 4c** and **4d**). The S content of CdS/3LG increases from 25.42% to 29.11% (integrated areas of XPS spectra in **Figure 4b** and **4c**) after irradiation for 30 min. However, such an increase from 30 min to 60 min is retarded (*i.e.*, from 29.11% to 29.57%; areas in **Figure 4c** and **4d**). This may be attributed to the fact that instead of diffusing into the solution, S is localized at the location where it is formed due to the covering by graphene, thereby leading to a slowdown of oxidation reaction as described in equation 2. Consequently, the photocorrosion resistance of CdS film is considerably improved when it is separated from the ambient environment by graphene.

As noted above, highly impermeable graphene physically prevents CdS from contacting with O_2 and H_2O. The DFT calculations were conducted to quantify the barrier potential imposed by graphene and identify if there exist the possibilities for O_2 and H_2O molecules to penetrate graphene (**Figure 5**). When an O_2 molecule approaches different sites (*i.e.*, bridge and hollow sites as illustrated in **Figure 5a**) on a monolayer of graphene possessing perfect carbon lattices, the barrier energies for O_2 molecule to perpendicularly go through the bridge and hollow sites are 111.2 eV and 37.4 eV, respectively, suggesting that the passage of O_2 over defect-free graphene will be completely blocked due to the steric hindrance effect.[39] More importantly, the impermeability of defective graphene *(i.e.*, divacancy) is also considered. When an O_2 molecule tends to pass normally through the central divacancy of graphene, the barrier energy is 13.9 eV, which is also indicative of impossible passage of an O_2 molecule through graphene (**Figure 5b**). Subsequently, the defective site is further expanded to an eight-atom vacancy, and a barrier energy of 0.32 eV is found, which is still too high for an O_2 molecule to penetrate graphene (**Figure 5b**).[40] Similar calculations are performed to simulate the possibilities for a H_2O molecular to migrate through a graphene barrier. Compared with O_2, H_2O is a polar molecule. In this case, different orientations of H_2O molecule (*i.e.,* either O atom or H atom facing the vacancy) passing through the graphene plane are simulated to identify the lower barrier energy. As evidenced in **Figure 5c**, similar to the case of O_2, the passage of a H_2O molecule through bridge site and hollow site on a monolayer of defect-free graphene is prohibited. Likewise, despite that the defects increase from divacancy to eight-atom vacancy, the penetration of a H_2O molecule over graphene via these defects is not possible (**Figure 5d**). Clearly, these calculations corrobor-

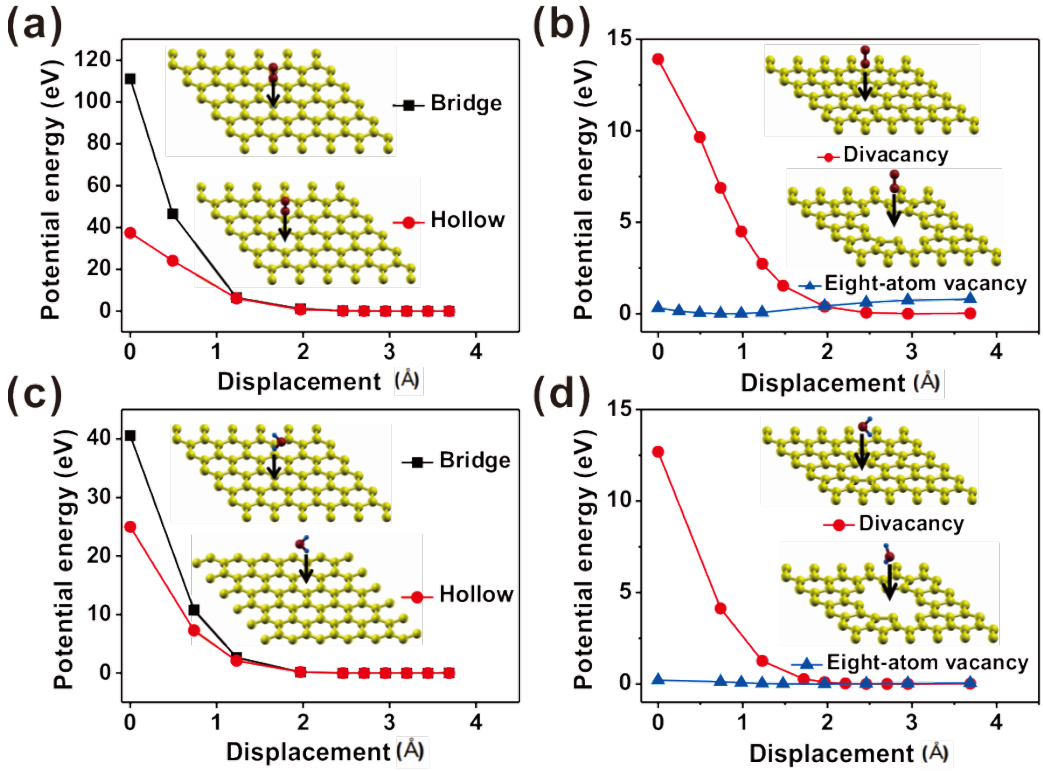

Figure 5. DFT calculations of an O2 molecule and a H2O molecule that intend to pass through a monolayer of graphene, respectively. Potential barrier of an O2 molecule passing through (a) graphene with perfect carbon lattices, and (b) the defective graphene, that is, possessing divacancy and eight-atom vacancy. Potential barrier of a H2O molecule diffusing through (c) graphene with perfect carbon lattices, and (d) the defective graphene.

ate that the migration of O_2 and H_2O molecules over monolayer graphene with vacancies is energetically unfavorable. Therefore, bilayer and trilayer graphene are expected to exhibit better impermeability performance.

Conclusion

In summary, we develop a viable route to effectively enhance the photocorrosion resistance and photocatalytic properties of efficient yet intrinsically non-photostable semiconductors via draping ultrathin graphene with a proper number of layers over them. In this study, CdS is chosen as the model semiconductor photocatalyst. Quite intriguingly, the lifetime of CdS/3LG electrode is increased by 8 times in comparison to as-prepared CdS electrode. The PL and EIS measurements suggest that after draping graphene over CdS electrode, the photogenerated electrons and holes of CdS can be effectively separated and participate in the photocatalytic reactions. As a result, the photocatalytic performance of CdS is markedly improved. A 2.5-fold increase in photocatalytic degradation efficiency is achieved by employing CdS/3LG over that using as-prepared CdS. More importantly, the DFT calculations reveal the robustness of graphene in sequestering the direct interaction of CdS with O_2 and H_2O from the ambient environment, providing insight into the anti-photocorrosion mechanism of graphene for improved photocatalysis. As such, this simple yet effective strategy renders the enhanced photocorrosion resistance and photocatalytic performance of CdS and can be easily extended to other semiconductors for potential applications in wastewater treatment, water splitting, and organic fuels production.

ASSOCIATED CONTENT

Supporting Information.
This material is available free of charge via the Internet at http://pubs.acs.org.

More characterization results

AUTHOR INFORMATION

Corresponding Author

*ychai@polyu.edu.hk (Y. Chai)

Notes

The authors declare no competing financial interest.

ACKNOWLEDGMENT

This work was supported by the Research Grant Council of Hong Kong (Grant No.: PolyU 252001/14E) and the Hong Kong Polytechnic University (grant Nos.: 1-BBA3 and 1-ZVK1).

REFERENCES

(1) Meissner, D.; Benndorf, C.; Memming, R. *Appl. Surf. Sci.* **1987**, *27*, 423-436.

(2) Wang, T.; Luo, Z. B.; Li, C. C.; Gong, J. L. *Chem. Soc. Rev.* **2014**, *43*, 7469-7484.

(3) Wang, M. Y.; Ioccozia, J.; Sun, L.; Lin, C. J.; Lin, Z. Q. *Energy Environ. Sci.* **2014**, *7*, 2182-2202.
(4) Porras, J. A.; Mills, I. N.; Transue, W. J.; Bernhard, S. *J. Am. Chem. Soc.* **2016**, *138*, 9460-9472.
(5) Xu, Y.; Ye, Y.; Liu, T.; Wang, X.; Zhang, B.; Wang, M.; Han, H.; Li, C. *J. Am. Chem. Soc.* **2016**, *138*, 10726-10729.
(6) Wu, K.; Du, Y.; Tang, H.; Chen, Z.; Lian, T. *J. Am. Chem. Soc.* **2015**, *137*, 10224-10230.
(7) Chen, Y. W.; Prange, J. D.; Dühnen, S.; Park, Y.; Gunji, M.; Chidsey, C. E.; McIntyre, P. C. *Nat. Mater.* **2011**, *10*, 539-544.
(8) Chen, J. Z.; Wu, X. J.; Yin, L. S.; Li, B.; Hong, X.; Fan, Z. X.; Chen, B.; Xue, C.; Zhang, H. *Angew. Chem. Int. Edit.* **2015**, *54*, 1210-1214.
(9) Inoue, T.; Fujishima, A.; Konishi, S.; Honda, K. *Nature* **1979**, *277*, 637-638.
(10) Hu, J.; Liu, A.; Jin, H.; Ma, D.; Yin, D.; Ling, P.; Wang, S.; Lin, Z.; Wang, J. *J. Am. Chem. Soc.* **2015**, *137*, 11004-11010.
(11) Xie, Y. P.; Yu, Z. B.; Liu, G.; Ma, X. L.; Cheng, H. M. *Energy Environ. Sci.* **2014**, *7*, 1895-1901.
(12) Wu, K. F.; Chen, Z. Y.; Lv, H. J.; Zhu, H. M.; Hill, C. L.; Lian, T. Q. *J. Am. Chem. Soc.* **2014**, *136*, 7708-7716.
(13) Tada, H.; Mitsui, T.; Kiyonaga, T.; Akita, T.; Tanaka, K. *Nat. Mater.* **2006**, *5*, 782-786.
(14) Li, J. T.; Cushing, S. K.; Zheng, P.; Senty, T.; Meng, F. K.; Bristow, A. D.; Manivannan, A.; Wu, N. Q. *J. Am. Chem. Soc.* **2014**, *136*, 8438-8449.
(15) El-Kady, M. F.; Strong, V.; Dubin, S.; Kaner, R. B. *Science* **2012**, *335*, 1326-1330.
(16) Wang, F.; Zhang, Y. B.; Tian, C. S.; Girit, C.; Zettl, A.; Crommie, M.; Shen, Y. R. *Science* **2008**, *320*, 206-209.
(17) Kim, K. S.; Zhao, Y.; Jang, H.; Lee, S. Y.; Kim, J. M.; Kim, K. S.; Ahn, J.-H.; Kim, P.; Choi, J.-Y.; Hong, B. H. *Nature* **2009**, *457*, 706-710.
(18) Shen, L. T.; Zhao, Y. D.; Wang, Y.; Song, R. B.; Yao, Q.; Chen, S. S.; Chai, Y. *J. Mater. Chem. A* **2016**, *4*, 5044-5050.
(19) Zhao, Y. D.; Xie, Y. Z.; Liu, Z. K.; Wang, X. S.; Chai, Y.; Yan, F. *Small* **2014**, *10*, 4521-4542.
(20) Zhao, Y. D.; Xie, Y. Z.; Bao, Z. Y.; Tsang, Y. H.; Xie, L. M.; Chai, Y. *J. Phys. Chem. C* **2014**, *118*, 11827-11832.
(21) Zhao, Y. D.; Xie, Y. Z.; Hui, Y. Y.; Tang, L. B.; Jie, W. J.; Jiang, Y. F.; Xu, L.; Lau, S. P.; Chai, Y. *J. Mater. Chem. C* **2013**, *1*, 4956-4961.
(22) Yin, Z. Y.; Zhu, J. X.; He, Q. Y.; Cao, X. H.; Tan, C. L.; Chen, H. Y.; Yan, Q. Y.; Zhang, H. *Adv. Energy Mater.* **2014**, *4*, 1300574.
(23) Huang, X.; Zeng, Z.; Fan, Z.; Liu, J.; Zhang, H. *Adv. Mater.* **2012**, *24*, 5979-6004.
(24) Nair, R. R.; Blake, P.; Grigorenko, A. N.; Novoselov, K. S.; Booth, T. J.; Stauber, T.; Peres, N. M. R.; Geim, A. K. *Science* **2008**, *320*, 1308-1308.
(25) Yin, P. T.; Shah, S.; Chhowalla, M.; Lee, K.-B. *Chem. Rev.* **2015**, *115*, 2483-2531.
(26) Berry, V. *Carbon* **2013**, *62*, 1-10.
(27) Zhao, Y.; Liu, Z.; Sun, T.; Zhang, L.; Jie, W.; Wang, X.; Xie, Y.; Tsang, Y. H.; Long, H.; Chai, Y. *ACS nano* **2014**, *8*, 12601-12611.
(28) Xie, K.; Wu, Z.; Wang, M.; Yu, J.; Gong, C.; Sun, L.; Lin, C. *Electrochem. Commun.* **2016**, *63*, 56-59.
(29) Perdew, J. P.; Burke, K.; Ernzerhof, M. *Phys. Rev. Lett.* **1996**, *77*, 3865-3868.
(30) Rengaraj, S.; Venkataraj, S.; Jee, S. H.; Kim, Y.; Tai, C. W.; Repo, E.; Koistinen, A.; Ferancova, A.; Sillanpaa, M. *Langmuir* **2011**, *27*, 352-358.
(31) Arguello, C.; Rousseau, D. L.; Porto, S. P. d. S. *Phys. Rev.* **1969**, *181*, 1351-1363.
(32) Sivasubramanian, V.; Arora, A.; Premila, M.; Sundar, C.; Sastry, V. *Physica E* **2006**, *31*, 93-98.
(33) Sun, Z.; Yan, Z.; Yao, J.; Beitler, E.; Zhu, Y.; Tour, J. M. *Nature* **2010**, *468*, 549-552.
(34) Ferrari, A. C.; Basko, D. M. *Nat. Nanotechnol.* **2013**, *8*, 235-246.
(35) Zhou, H. Q.; Qiu, C. Y.; Liu, Z.; Yang, H. C.; Hu, L. J.; Liu, J.; Yang, H. F.; Gu, C. Z.; Sun, L. F. *J. Am. Chem. Soc.* **2010**, *132*, 944-946.
(36) Ho, P. H.; Chen, C. H.; Shih, F. Y.; Chang, Y. R.; Li, S. S.; Wang, W. H.; Shih, M. C.; Chen, W. T.; Chiu, Y. P.; Li, M. K.; Shih, Y. S.; Chen, C. W. *Adv. Mater.* **2015**, *27*, 7809-7815.
(37) Bai, S.; Ge, J.; Wang, L. L.; Gong, M.; Deng, M. S.; Kong, Q.; Song, L.; Jiang, J.; Zhang, Q.; Luo, Y.; Xie, Y.; Xiong, Y. J. *Adv. Mater.* **2014**, *26*, 5689-5695.
(38) Meissner, D.; Memming, R.; Kastening, B. *J. Phys. Chem.* **1988**, *92*, 3476-3483.
(39) Yao, F.; Güneş, F.; Ta, H. Q.; Lee, S. M.; Chae, S. J.; Sheem, K. Y.; Cojocaru, C. S.; Xie, S. S.; Lee, Y. H. *J. Am. Chem. Soc.* **2012**, *134*, 8646-8654.
(40) Mehmood, F.; Pachter, R.; Lu, W. J.; Boeckl, J. J. *J. Phys. Chem. C* **2013**, *117*, 10366-10374.

Insert Table of Contents artwork here